ARTICLE

The Improved Element-Free Galerkin Method for Anisotropic Steady-State Heat Conduction Problems

Heng Cheng[1], Zebin Xing[1] and Miaojuan Peng[2,*]

[1]School of Applied Science, Taiyuan University of Science and Technology, Taiyuan, 030024, China

[2]Department of Civil Engineering, School of Mechanics and Engineering Science, Shanghai University, Shanghai, 200444, China

*Corresponding Author: Miaojuan Peng. Email: mjpeng@shu.edu.cn

ABSTRACT

In this paper, we considered the improved element-free Galerkin (IEFG) method for solving 2D anisotropic steady-state heat conduction problems. The improved moving least-squares (IMLS) approximation is used to establish the trial function, and the penalty method is applied to enforce the boundary conditions, thus the final discretized equations of the IEFG method for anisotropic steady-state heat conduction problems can be obtained by combining with the corresponding Galerkin weak form. The influences of node distribution, weight functions, scale parameters and penalty factors on the computational accuracy of the IEFG method are analyzed respectively, and these numerical solutions show that less computational resources are spent when using the IEFG method.

1 Introduction

Heat conduction in anisotropic material has been widely applied in various branches of science and engineering. Unlike those of isotropic materials, the thermal conductivity of anisotropic materials varies with direction. Due to the complexity of such problems, analytical solutions are limited to only a few idealized cases. Therefore, how to obtain the internal temperature distribution of anisotropic materials effectively and accurately is one of the significant directions in scientific research.

Currently, lots of meshless methods have been applied for researching heat conduction in anisotropic materials, such as local meshless method [1], regularized meshless method [2], radial basis integral equation method [3], meshless singular boundary method [4], radial basis function method [5], and so on. Compared with the traditional finite element method, a meshless method [6–9] needs only the distribution of discrete nodes, which can avoid the meshing-related drawbacks. Thus, the great precision of numerical solutions can be obtained.

As an important meshless method, the EFG method [10] was studied in 1994, in this method, the shape function was constructed by using the MLS approximation [11]. However, the disadvantage of the singular matrix often occurs in this method.

In order to eliminate the singular matrices, Cheng et al. studied the IMLS approximation [12] in 2003, thus the IEFG method was applied for many problems, such as advection-diffusion [13], elastoplasticity [14], diffusional drug release [15] problems, and so on. Under the similar computational accuracy, the IEFG method has the advantage of higher calculation speed.

By introducing the singular weight function into the MLS approximation, Lancaster et al. studied the interpolating MLS method [11], thus the boundary condition can be enforced directly in corresponding meshless method. Ren et al. improved the interpolating MLS method [16], thus the corresponding interpolating EFG method was presented [17]. Additionally, some mechanics problems [18–20] were analyzed by using this method. Qin et al. developed the interpolating smoothed particle method [21].

Using the nonsingular weight function, Wang et al. developed the improved interpolating MLS method, using this method to construct the trial function, thus the improved interpolating EFG method are presented [22], and some large deformation problems [23–25] were analyzed by using this method.

By combining the traditional finite difference method with various kinds of meshless methods, thus the hybrid EFG method [26–29], the dimensional splitting complex variable EFG method [30–34], the dimension split reproducing kernel particle method [35–38] and the hybrid generalized interpolated EFG method [39] are proposed respectively, these methods can solve the multi-dimensional problems efficiently.

In this study, the IEFG method is used for solving anisotropic steady-state heat conduction problem. The shape functions are established by using the IMLS approximation, using the penalty method to enforce the boundary condition, thus the final formulae of discretized equations of the IEFG method for anisotropic steady-state heat conduction problem can be derived by combining with the corresponding Galerkin weak form.

The influences of nodes number, weight functions, scale parameters and penalty factors on computational accuracy of the IEFG method are discussed by given examples, and numerical solutions show that the IEFG method for anisotropic steady-state heat conduction problems is convergent, compared with the traditional EFG method, less computational resources are spent when using the IEFG method.

2 The IMLS Approximation

For an arbitrary function $u(\boldsymbol{x})$, the approximation is

$$u^h(\boldsymbol{x}) = \sum_{i=1}^{m} p_i(\boldsymbol{x}) \cdot a_i(\boldsymbol{x}) = \boldsymbol{p}^{\mathrm{T}}(\boldsymbol{x}) \cdot \boldsymbol{a}(\boldsymbol{x}), (\boldsymbol{x} \in \Omega), \tag{1}$$

where $\boldsymbol{p}^{\mathrm{T}}(\boldsymbol{x})$ is basis function vector, m is basis function number, and

$$\boldsymbol{a}^{\mathrm{T}}(\boldsymbol{x}) = (a_1(\boldsymbol{x}), a_2(\boldsymbol{x}), \cdots, a_m(\boldsymbol{x})) \tag{2}$$

is coefficient vector of $\boldsymbol{p}^{\mathrm{T}}(\boldsymbol{x})$.

In general,

$$\boldsymbol{p}^{\mathrm{T}}(\boldsymbol{x}) = (1, x_1, x_2, x_3), \tag{3}$$

$$\boldsymbol{p}^{\mathrm{T}}(\boldsymbol{x}) = (1, x_1, x_2, x_3, x_1^2, x_2^2, x_3^2, x_1 x_2, x_2 x_3, x_1 x_3). \tag{4}$$

The local approximation is

$$u^h(\boldsymbol{x}, \hat{\boldsymbol{x}}) = \sum_{i=1}^{m} p_i(\hat{\boldsymbol{x}}) \cdot a_i(\boldsymbol{x}) = \boldsymbol{p}^{\mathrm{T}}(\hat{\boldsymbol{x}}) \cdot \boldsymbol{a}(\boldsymbol{x}). \tag{5}$$

Define

$$J = \sum_{I=1}^{n} w(\boldsymbol{x} - \boldsymbol{x}_I)[u^h(\boldsymbol{x}, \boldsymbol{x}_I) - u_I]^2 = \sum_{I=1}^{n} w(\boldsymbol{x} - \boldsymbol{x}_I) \left[\sum_{i=1}^{m} p_i(\boldsymbol{x}_I) \cdot a_i(\boldsymbol{x}) - u_I \right]^2, \tag{6}$$

where $w(\boldsymbol{x} - \boldsymbol{x}_I)$ is a weighting function, and $\boldsymbol{x}_I \ (I = 1, 2, \cdots, n)$ are the nodes with influence domains covering the point $\boldsymbol{x}$.

Eq. (6) can be written as

$$J = (\boldsymbol{P}a - \boldsymbol{u})^{\mathrm{T}} \boldsymbol{W}(\boldsymbol{x})(\boldsymbol{P}a - \boldsymbol{u}), \tag{7}$$

where

$$\boldsymbol{u}^{\mathrm{T}} = (u_1, u_2, \cdots, u_n), \tag{8}$$

$$\boldsymbol{P} = \begin{bmatrix} p_1(\boldsymbol{x}_1) & p_2(\boldsymbol{x}_1) & \cdots & p_m(\boldsymbol{x}_1) \\ p_1(\boldsymbol{x}_2) & p_2(\boldsymbol{x}_2) & \cdots & p_m(\boldsymbol{x}_2) \\ \vdots & \vdots & \ddots & \vdots \\ p_1(\boldsymbol{x}_n) & p_2(\boldsymbol{x}_n) & \cdots & p_m(\boldsymbol{x}_n) \end{bmatrix}, \tag{9}$$

and

$$\boldsymbol{W}(\boldsymbol{x}) = \begin{bmatrix} w(\boldsymbol{x} - \boldsymbol{x}_1) & 0 & \cdots & 0 \\ 0 & w(\boldsymbol{x} - \boldsymbol{x}_2) & \cdots & 0 \\ \vdots & \vdots & \ddots & \vdots \\ 0 & 0 & \cdots & w(\boldsymbol{x} - \boldsymbol{x}_n) \end{bmatrix}. \tag{10}$$

From

$$\frac{\partial J}{\partial \boldsymbol{a}} = \boldsymbol{A}(\boldsymbol{x})\boldsymbol{a}(\boldsymbol{x}) - \boldsymbol{B}(\boldsymbol{x})\boldsymbol{u} = 0, \tag{11}$$

we have

$$\boldsymbol{A}(\boldsymbol{x})\boldsymbol{a}(\boldsymbol{x}) = \boldsymbol{B}(\boldsymbol{x})\boldsymbol{u}, \tag{12}$$

where

$$\boldsymbol{A}(\boldsymbol{x}) = \boldsymbol{P}^{\mathrm{T}} \boldsymbol{W}(x)\boldsymbol{P}, \tag{13}$$

$$\boldsymbol{B}(\boldsymbol{x}) = \boldsymbol{P}^{\mathrm{T}} \boldsymbol{W}(x). \tag{14}$$

Eq. (12) sometimes forms singular or ill-conditional matrix. In order to make up for this deficiency, for basis functions

$$\boldsymbol{q} = (q_i) = (1, x_1, x_2, x_3, x_1^2, x_2^2, x_3^2, x_1 x_2, x_2 x_3, x_3 x_1, \cdots), \tag{15}$$

using Gram-Schmidt process, we can obtain

$$p_i = q_i - \sum_{k=1}^{i-1} \frac{(q_i, p_k)}{(p_k, p_k)} p_k, \ (i = 1, 2, 3, \cdots), \tag{16}$$

and

$$(p_i, p_j) = 0, (i \neq j). \tag{17}$$

Then from Eq. (12), $a(x)$ can be obtained

$$a(x) = A^*(x)B(x)u, \tag{18}$$

where

$$A^*(x) = \begin{bmatrix} \dfrac{1}{(p_1, p_1)} & 0 & \cdots & 0 \\ 0 & \dfrac{1}{(p_2, p_2)} & 0 & 0 \\ \vdots & \vdots & \ddots & \vdots \\ 0 & 0 & \cdots & \dfrac{1}{(p_n, p_n)} \end{bmatrix}. \tag{19}$$

Substituting Eq. (18) into Eq. (5), we have

$$u^h(x) = \boldsymbol{\Phi}^*(x)u = \sum_{I=1}^{n} \Phi_I^*(x)u_I, \tag{20}$$

where

$$\boldsymbol{\Phi}^*(x) = (\Phi_1^*(x), \Phi_2^*(x), \cdots, \Phi_n^*(x)) = \boldsymbol{p}^{\mathrm{T}}(x)A^*(x)B(x) \tag{21}$$

is the shape function.

This is the IMLS approximation [12].

3 The IEFG Method for 2D Anisotropic Steady-State Heat Conduction Problems

The governing equation is

$$k_{11} \frac{\partial^2 u(x)}{\partial x_1^2} + k_{22} \frac{\partial^2 u(x)}{\partial x_2^2} + k_{12} \frac{\partial^2 u(x)}{\partial x_1 \partial x_2} + k_{21} \frac{\partial^2 u(x)}{\partial x_2 \partial x_1} + f(x) = 0, (x = (x_1, x_2) \in \Omega), \tag{22}$$

the boundary conditions are

$$u(x) = \bar{u}(x), \ (x \in \Gamma_u), \tag{23}$$

$$q(x) = k_{11} \frac{\partial u(x)}{\partial x_1} n_1 + k_{12} \frac{\partial u(x)}{\partial x_2} n_1 + k_{22} \frac{\partial u(x)}{\partial x_2} n_2 + k_{21} \frac{\partial u(x)}{\partial x_1} n_2 = \bar{q}(x), (x \in \Gamma_q), \tag{24}$$

where k_{ij} $(i, j = 1, 2)$ are the thermal conductivity coefficients, $u(x)$ is the unknown temperature function, $f(x)$ is the internal heat source generation rate, $\bar{u}$ and $\bar{q}$ are the given temperatures, $\Gamma = \Gamma_u \cup \Gamma_q$, $\Gamma_u \cap \Gamma_q = \emptyset$, n_i $(i = 1, 2)$ is the unit outward normal to boundary Γ in direction x_i. According to the thermodynamic principles and Onsagar's reciprocity relation [40,41], the conductivity coefficients must satisfy

$$k_{11} > 0; k_{22} > 0; k_{12} = k_{21}; k_{11}k_{22} > k_{12}^2.$$

The equivalent functional of anisotropic steady-state heat conduction problems is

$$\Pi = \int_{\Omega} \frac{1}{2} \left[k_{11} \left(\frac{\partial u}{\partial x_1} \right)^2 + k_{22} \left(\frac{\partial u}{\partial x_2} \right)^2 + 2k_{12} \frac{\partial u}{\partial x_1} \frac{\partial u}{\partial x_2} \right] \mathrm{d}\Omega - \int_{\Omega} u f \mathrm{d}\Omega - \int_{\Gamma_q} u \bar{q} \mathrm{d}\Gamma. \tag{25}$$

By applying the penalty method to enforce the boundary conditions, we can obtain

$$\Pi^* = \Pi + \frac{\alpha}{2} \int_{\Gamma_u} (u - \bar{u})(u - \bar{u}) \mathrm{d}\Gamma, \tag{26}$$

where α refer to penalty factor.

Let

$$\delta \Pi^* = 0, \tag{27}$$

the following weak form can be obtained

$$\int_{\Omega} \delta (L_1 u)^{\mathrm{T}} \cdot (L_2 u) \mathrm{d}\Omega - \int_{\Omega} \delta u \cdot f \mathrm{d}\Omega - \int_{\Gamma_q} \delta u \cdot \bar{q} \mathrm{d}\Gamma + \alpha \int_{\Gamma_u} \delta u \cdot u \mathrm{d}\Gamma - \alpha \int_{\Gamma_u} \delta u \cdot \bar{u} \mathrm{d}\Gamma = 0, \tag{28}$$

where

$$L_1(\cdot) = \begin{bmatrix} \sqrt{k_{11}} \cdot \frac{\partial}{\partial x_1} \\ \sqrt{k_{22}} \cdot \frac{\partial}{\partial x_2} \\ \sqrt{2k_{12}} \cdot \frac{\partial}{\partial x_1} \end{bmatrix} (\cdot), \tag{29}$$

$$L_2(\cdot) = \begin{bmatrix} \sqrt{k_{11}} \cdot \frac{\partial}{\partial x_1} \\ \sqrt{k_{22}} \cdot \frac{\partial}{\partial x_2} \\ \sqrt{2k_{12}} \cdot \frac{\partial}{\partial x_2} \end{bmatrix} (\cdot). \tag{30}$$

In the problem domain, we select M nodes x_I ($I = 1, 2, \cdots, M$), and the corresponding function is

$$u_I = u(x_I). \tag{31}$$

From the IMLS approximation, we can obtain

$$u^h(x) = \boldsymbol{\Phi}^*(x) u = \sum_{I=1}^{n} \Phi_I^*(x) u_I, \tag{32}$$

where

$$u = (u_1, u_2, \cdots, u_n)^{\mathrm{T}}. \tag{33}$$

From Eqs. (29), (30) and (32), we have

$$L_1 u(x) = \sum_{I=1}^{n} \begin{bmatrix} \sqrt{k_{11}} \cdot \frac{\partial}{\partial x_1} \\ \sqrt{k_{22}} \cdot \frac{\partial}{\partial x_2} \\ \sqrt{2k_{12}} \cdot \frac{\partial}{\partial x_1} \end{bmatrix} \Phi_I^*(x) u_I = \sum_{I=1}^{n} B_{1I}(x) u_I = B_1(x) u, \tag{34}$$

$$L_2 u(x) = \sum_{I=1}^{n} \begin{bmatrix} \sqrt{k_{11}} \cdot \frac{\partial}{\partial x_1} \\ \sqrt{k_{22}} \cdot \frac{\partial}{\partial x_2} \\ \sqrt{2k_{12}} \cdot \frac{\partial}{\partial x_2} \end{bmatrix} \Phi_I^*(x) u_I = \sum_{I=1}^{n} B_{2I}(x) u_I = B_2(x) u, \tag{35}$$

where

$$\boldsymbol{B}_1(\boldsymbol{x}) = (\boldsymbol{B}_{11}(\boldsymbol{x}), \boldsymbol{B}_{12}(\boldsymbol{x}), \cdots, \boldsymbol{B}_{1n}(\boldsymbol{x})),$$ (36)

$$\boldsymbol{B}_2(\boldsymbol{x}) = (\boldsymbol{B}_{21}(\boldsymbol{x}), \boldsymbol{B}_{22}(\boldsymbol{x}), \cdots, \boldsymbol{B}_{2n}(\boldsymbol{x})),$$ (37)

$$\boldsymbol{B}_{1I}(\boldsymbol{x}) = \begin{bmatrix} \sqrt{k_{11}} \cdot \Phi_{I,1}^*(\boldsymbol{x}) \\ \sqrt{k_{22}} \cdot \Phi_{I,2}^*(\boldsymbol{x}) \\ \sqrt{2k_{12}} \cdot \Phi_{I,1}^*(\boldsymbol{x}) \end{bmatrix},$$ (38)

$$\boldsymbol{B}_{2I}(\boldsymbol{x}) = \begin{bmatrix} \sqrt{k_{11}} \cdot \Phi_{I,1}^*(\boldsymbol{x}) \\ \sqrt{k_{22}} \cdot \Phi_{I,2}^*(\boldsymbol{x}) \\ \sqrt{2k_{12}} \cdot \Phi_{I,2}^*(\boldsymbol{x}) \end{bmatrix}.$$ (39)

Substituting Eqs. (32), (34) and (35) into Eq. (28) yields

$$\int_\Omega \delta[\boldsymbol{B}_1(\boldsymbol{x})\boldsymbol{u}]^{\mathrm{T}} \cdot [\boldsymbol{B}_2(\boldsymbol{x})\boldsymbol{u}] \mathrm{d}\Omega - \int_\Omega \delta[\boldsymbol{\Phi}^*(\boldsymbol{x})\boldsymbol{u}]^{\mathrm{T}} \cdot f \mathrm{d}\Omega - \int_{\Gamma_q} \delta[\boldsymbol{\Phi}^*(\boldsymbol{x})\boldsymbol{u}]^{\mathrm{T}} \cdot \bar{q} \mathrm{d}\Gamma \\ + \alpha \int_{\Gamma_u} \delta[\boldsymbol{\Phi}^*(\boldsymbol{x})\boldsymbol{u}]^{\mathrm{T}} \cdot [\boldsymbol{\Phi}^*(\boldsymbol{x})\boldsymbol{u}] \mathrm{d}\Gamma - \alpha \int_{\Gamma_u} \delta[\boldsymbol{\Phi}^*(\boldsymbol{x})\boldsymbol{u}]^{\mathrm{T}} \cdot \bar{u} \mathrm{d}\Gamma = 0.$$ (40)

Analyzing all terms in Eq. (40), respectively, we can obtain

$$\int_\Omega \delta[\boldsymbol{B}_1(\boldsymbol{x})\boldsymbol{u}]^{\mathrm{T}} \cdot [\boldsymbol{B}_2(\boldsymbol{x})\boldsymbol{u}] \mathrm{d}\Omega = \delta\boldsymbol{u}^{\mathrm{T}} \cdot \left[\int_\Omega \boldsymbol{B}_1^{\mathrm{T}}(\boldsymbol{x})\boldsymbol{B}_2(\boldsymbol{x}) \mathrm{d}\Omega \right] \cdot \boldsymbol{u},$$ (41)

$$\int_\Omega \delta[\boldsymbol{\Phi}^*(\boldsymbol{x})\boldsymbol{u}]^{\mathrm{T}} \cdot f \mathrm{d}\Omega = \delta\boldsymbol{u}^{\mathrm{T}} \cdot \left[\int_\Omega \boldsymbol{\Phi}^{*\mathrm{T}}(\boldsymbol{x})f \mathrm{d}\Omega \right],$$ (42)

$$\int_{\Gamma_q} \delta[\boldsymbol{\Phi}^*(\boldsymbol{x})\boldsymbol{u}]^{\mathrm{T}} \cdot \bar{q} \mathrm{d}\Gamma = \delta\boldsymbol{u}^{\mathrm{T}} \cdot \left[\int_{\Gamma_q} \boldsymbol{\Phi}^{*\mathrm{T}}(\boldsymbol{x})\bar{q} \mathrm{d}\Gamma \right],$$ (43)

$$\alpha \int_{\Gamma_u} \delta[\boldsymbol{\Phi}^*(\boldsymbol{x})\boldsymbol{u}]^{\mathrm{T}} \cdot [\boldsymbol{\Phi}^*(\boldsymbol{x})\boldsymbol{u}] \mathrm{d}\Gamma = \delta\boldsymbol{u}^{\mathrm{T}} \cdot \left[\alpha \int_{\Gamma_u} \boldsymbol{\Phi}^{*\mathrm{T}}(\boldsymbol{x})\boldsymbol{\Phi}^*(\boldsymbol{x}) \mathrm{d}\Gamma \right] \cdot \boldsymbol{u},$$ (44)

$$\alpha \int_{\Gamma_u} \delta[\boldsymbol{\Phi}^*(\boldsymbol{x})\boldsymbol{u}]^{\mathrm{T}} \cdot \bar{u} \mathrm{d}\Gamma = \delta\boldsymbol{u}^{\mathrm{T}} \cdot \left[\alpha \int_{\Gamma_u} \boldsymbol{\Phi}^{*\mathrm{T}}(\boldsymbol{x})\bar{u} \mathrm{d}\Gamma \right].$$ (45)

Let

$$\boldsymbol{K} = \int_\Omega \boldsymbol{B}_1^{\mathrm{T}}(\boldsymbol{x})\boldsymbol{B}_2(\boldsymbol{x}) \mathrm{d}\Omega,$$ (46)

$$\boldsymbol{F}_1 = \int_\Omega \boldsymbol{\Phi}^{*\mathrm{T}}(\boldsymbol{x})f \mathrm{d}\Omega,$$ (47)

$$\boldsymbol{F}_2 = \int_{\Gamma_q} \boldsymbol{\Phi}^{*\mathrm{T}}(\boldsymbol{x})\bar{q} \mathrm{d}\Gamma,$$ (48)

$$\boldsymbol{K}_\alpha = \alpha \int_{\Gamma_u} \boldsymbol{\Phi}^{*\mathrm{T}}(\boldsymbol{x})\boldsymbol{\Phi}^*(\boldsymbol{x}) \mathrm{d}\Gamma,$$ (49)

$$\boldsymbol{F}_\alpha = \alpha \int_{\Gamma_u} \boldsymbol{\Phi}^{*\mathrm{T}}(\boldsymbol{x})\bar{u} \mathrm{d}\Gamma.$$ (50)

Substituting Eqs. (41)–(45) into Eq. (40), we have

$$\delta\boldsymbol{u}^{\mathrm{T}} \cdot (\boldsymbol{K}\boldsymbol{u} + \boldsymbol{K}_\alpha \boldsymbol{u} - \boldsymbol{F}_1 - \boldsymbol{F}_2 - \boldsymbol{F}_\alpha) = 0,$$ (51)

the δu^{T} is arbitrary, then we can obtain

$$\hat{K}u = \hat{F}, \tag{52}$$

where

$$\hat{K} = K + K_\alpha, \tag{53}$$

$$\hat{F} = F_1 + F_2 + F_\alpha. \tag{54}$$

This is the IEFG method for 2D anisotropic steady-state heat conduction problem.

4 Numerical Examples

The formula of the relative error is

$$||u - u^h||_{L^2(\Omega)}^{rel} = \frac{||u - u^h||_{L^2(\Omega)}}{||u||_{L^2(\Omega)}}, \tag{55}$$

where

$$||u - u^h||_{L^2(\Omega)} = \left(\int_\Omega (u - u^h)^2 \mathrm{d}\Omega \right)^{1/2}. \tag{56}$$

For simplicity, we select linear basis function in this section, and 4×4 Gaussian points are selected in each integral grid. Fourth numerical examples are presented, and the IEFG and the EFG methods are used to solve them, respectively.

The first example is

$$5\frac{\partial^2 u(\mathbf{x})}{\partial x_1^2} + \frac{\partial^2 u(\mathbf{x})}{\partial x_2^2} + 4\frac{\partial^2 u(\mathbf{x})}{\partial x_1 \partial x_2} = 0, (\mathbf{x} = (x_1, x_2) \in \Omega), \tag{57}$$

the boundary conditions are

$$u(0, x_2) = x_2^3/3, \tag{58}$$

$$u(1, x_2) = 1/5 - x_2 + x_2^2 + x_2^3/3, \tag{59}$$

$$u(x_1, 0) = x_1^3/5, \tag{60}$$

$$u(x_1, 1) = x_1^3/5 - x_1^2 + x_1 + 1/3. \tag{61}$$

The problem domain is $\Omega = [0, 1] \times [0, 1]$, and

$$u = x_1^3/5 - x_1^2 x_2 + x_1 x_2^2 + x_2^3/3 \tag{62}$$

is the exact solution.

In order to illustrate the advantages of the IEFG method for 2D anisotropic steady-state heat conduction problem, we should study the convergence of this method.

Using the IEFG method to solve it, the cubic spline weight function is selected, $d_{\max} = 1.19$, $\alpha = 6.0 \times 10^5$, Fig. 1 shows the relationship between relative errors of numerical solutions and nodes number. It is shown that, with the increase of nodes, the precision of numerical solutions will improve as well. Thus, the numerical solution of the IEFG method in this paper is convergent.
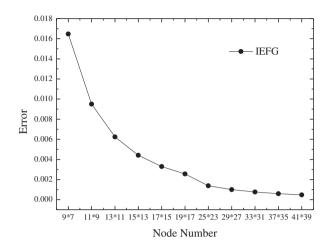
Figure 1: The error of numerical solutions of the IEFG method with the increase of nodes

The influences of weight function, scale parameter and penalty factor on solution of the IEFG method will be discussed, respectively.

1) Weighting function

If we select the cubic spline function, 17×15 regular nodes and 16×14 integral grids are selected respectively, $\alpha = 6.0 \times 10^5$, $d_{max} = 1.19$, thus the smaller relative error is 0.3292%. When the quartic spline function is used, same nodes and integral grids are used respectively, $\alpha = 4.0 \times 10^5$, $d_{max} = 1.15$, thus the smaller relative error is 0.3320%. It is shown that the relative error is slightly bigger when using the quartic spline function. In this section, we select the cubic spline function.

2) Scale parameter d_{max}

The same nodes and integral grids are used respectively, $\alpha = 4.0 \times 10^5$, and the cubic spline function is used. Fig. 2 shows the relationship between d_{max} and relative error. It is shown that, when $d_{max} = 1.19$, the smaller relative error is obtained.
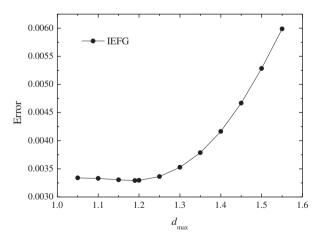

Figure 2: The error of numerical solutions of the IEFG method with the increase of d_{max}

3) Penalty factor α

The same nodes, integral grids and the weight function are used respectively, $d_{max} = 1.19$, Fig. 3 shows the relationship between α and relative error. It is shown that, when $\alpha = 1.0 \times 10^5 \sim 1.0 \times 10^6$, the smaller relative error is obtained.
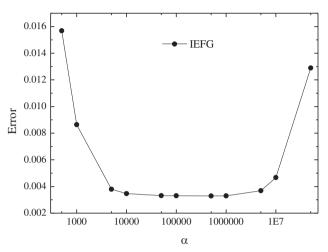

Figure 3: The error of numerical solutions of the IEFG method for different α

When the IEFG method is used to solve it, 17×15 regular nodes and 16×14 integral grids are selected, $d_{max} = 1.19$, $\alpha = 6.0 \times 10^5$, and the cubic spline weight function is used; when the EFG method is used, keep all parameters consistent with the IEFG method, thus the same computational accuracy can be obtained, and the relative errors of two methods are equal to 0.3292%.

Figs. 4–7 show the comparison of numerical results and analytical ones. It is shown that the numerical solutions of two methods are in agreement very well with analytical one. The CPU times of the EFG and the IEFG methods are 0.61 and 0.51 s, respectively. Compared with the EFG method, the calculation speed of the IEFG method is slightly faster.
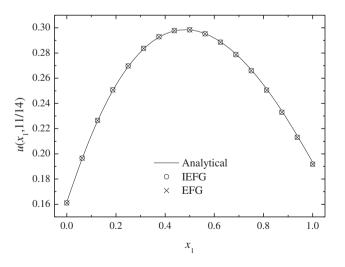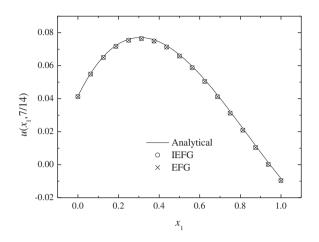

Figure 4: The comparison of numerical solutions and analytical ones along x_1-axis

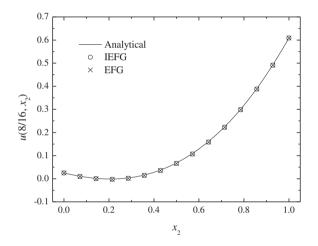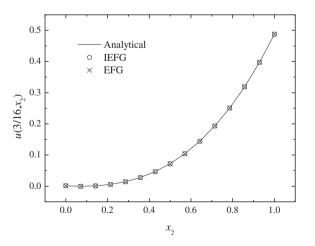**Figure 5:** The comparison of numerical solutions and analytical ones along x_1-axis

Figure 6: The comparison of numerical solutions and analytical ones along x_2-axis

Figure 7: The comparison of numerical solutions and analytical ones along x_2-axis

The second example we considered is an orthotropic medium, and the problem domain is a semi-circular ring, the outer and inner radii are 2 and 1, respectively. The governing equation is

$$\frac{\partial^2 u(\boldsymbol{x})}{\partial x_1^2} + 2\frac{\partial^2 u(\boldsymbol{x})}{\partial x_2^2} = 0, (\boldsymbol{x} = (x_1, x_2) \in \Omega), \tag{63}$$

the boundary conditions are

$$\frac{\partial u(x_1, 0)}{\partial x_2} = 0, (-2 \le x_1 \le -1, 1 \le x_1 \le 2); \tag{64}$$

$$u(x_1, x_2) = -x_1^2 + x_2^2/2, (\sqrt{x_1^2 + x_2^2} = 1, \sqrt{x_1^2 + x_2^2} = 2). \tag{65}$$

The problem domain is $\Omega = \{(x_1, x_2): 1 \le \sqrt{x_1^2 + x_2^2} \le 2, -2 \le x_1 \le -1, 1 \le x_1 \le 2\}$, and

$$u = -x_1^2 + x_2^2/2 \tag{66}$$

is the exact solution.

Using the IEFG method to solve it, 21×11 nodes (see Fig. 8) and 20×10 integral grids are selected respectively, $d_{max} = 1.7$, $\alpha = 1.0 \times 10^3$, and the cubic weight function is used, thus the smaller relative error is 0.0735%; when the EFG method is used to solve it, keep all parameters consistent with the IEFG method, thus the same calculation accuracy is obtained. The CPU times of the EFG and the IEFG methods are 1.5 and 1.1 s, respectively.
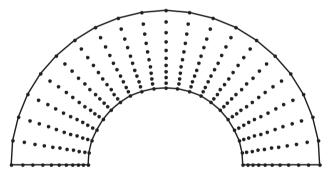

Figure 8: Nodes distributed on the problem domain

Figs. 9–12 show that the numerical results are in agreement very well with analytical one. Obviously, the advantage of the IEFG method is its faster calculation speed.

The third example is a heat conduction problem in orthotropic material with internal heat source

$$\frac{\partial^2 u(\boldsymbol{x})}{\partial x_1^2} + 4\frac{\partial^2 u(\boldsymbol{x})}{\partial x_2^2} + x_1 = 0, (\boldsymbol{x} = (x_1, x_2) \in \Omega), \tag{67}$$

the boundary conditions are

$$u(0, x_2) = 7/6, \tag{68}$$

$$u(1, x_2) = 1, \tag{69}$$

$$\frac{\partial u(x_1, 0)}{\partial x_2} = \frac{\partial u(x_1, 1)}{\partial x_2} = 0. \tag{70}$$

The problem domain is $\Omega = [0, 1] \times [0, 1]$, and

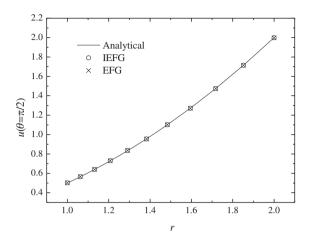$$u = 7/6 - x_1^3/6 \tag{71}$$

is the exact solution.

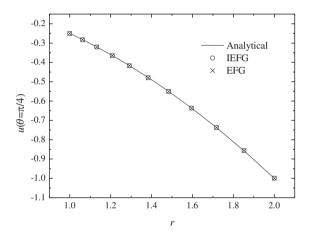**Figure 9:** The comparison of numerical solutions and analytical ones when $\theta = \pi/2$

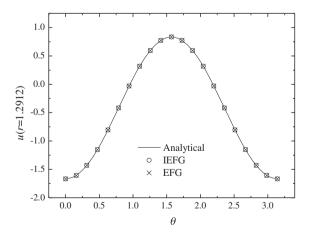**Figure 10:** The comparison of numerical solutions and analytical ones when $\theta = \pi/4$

Figure 11: The comparison of numerical solutions and analytical ones at the fifth node with the direction of r
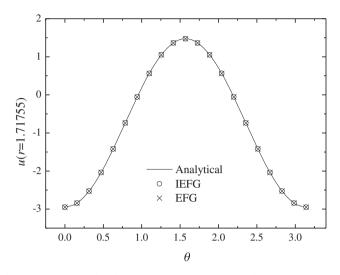
Figure 12: The comparison of numerical solutions and analytical ones at the ninth node with the direction of r

Using the IEFG method to solve it, 11×11 regular nodes and 10×10 integral grids are selected respectively, $d_{max} = 1.2$, $\alpha = 8.0 \times 10^3$, the cubic spline weight function is used; when the EFG method is used, keep all parameters consistent with the IEFG method, thus the relative errors of both methods are equal to 0.0019%.

Figs. 13–14 show the comparison of numerical solutions and analytical ones. It is shown that the numerical results are in agreement very well with analytical one. The CPU times of the EFG and the IEFG methods are 0.4 and 0.3 s, respectively. Obviously, the IEFG method has slightly faster calculation speed than the EFG method.
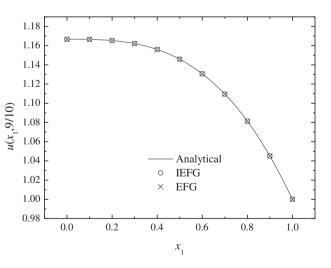

Figure 13: The comparison of numerical solutions and analytical ones along x_1-axis
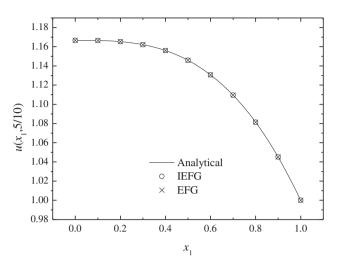
Figure 14: The comparison of numerical solutions and analytical ones along x_1-axis

The fourth example is

$$2\frac{\partial^2 u(\boldsymbol{x})}{\partial x_1^2} + 3\frac{\partial^2 u(\boldsymbol{x})}{\partial x_2^2} + 2\frac{\partial^2 u(\boldsymbol{x})}{\partial x_1 \partial x_2} = 0, (\boldsymbol{x} = (x_1, x_2) \in \Omega), \tag{72}$$

the boundary conditions are

$$u(0, x_2) = -x_2^2, \tag{73}$$

$$u(1, x_2) = 1 - x_2^2 + x_2, \tag{74}$$

$$u(x_1, 0) = x_1^2, \tag{75}$$

$$u(x_1, 1) = x_1^2 - 1 + x_1. \tag{76}$$

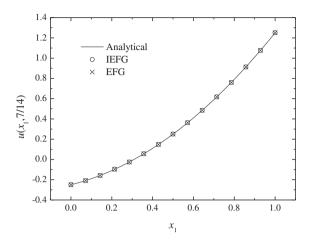The problem domain is $\Omega = [0, 1] \times [0, 1]$, and

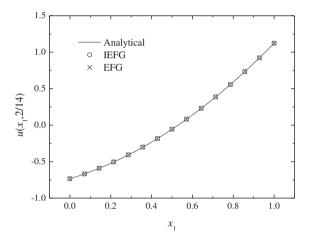$$u = x_1^2 - x_2^2 + x_1 x_2 \tag{77}$$

is the exact solution.

When the IEFG method is used to solve it, 15×15 regular nodes and 14×14 integral grids are selected, respectively, the cubic spline weight function is used, $d_{max} = 1.3, \alpha = 6.0 \times 10^3$, thus the relative error is 0.0517%; when the EFG method is used, keep all parameters consistent with the IEFG method, thus the same calculation accuracy is obtained.

Figs. 15–18 show the comparison of numerical solutions and analytical ones, it is shown that the numerical results are in agreement very well with analytical one. The CPU times of the EFG and the IEFG methods are 0.53 and 0.47 s, respectively. Thus, the IEFG method can solve it with less computational resources.

Figure 15: The comparison of numerical solutions and analytical ones along x_1-axis

Figure 16: The comparison of numerical solutions and analytical ones along x_1-axis

Figure 17: The comparison of numerical solutions and analytical ones along x_2-axis

Figure 18: The comparison of numerical solutions and analytical ones along x_2-axis

In order to compare the accuracy and efficiency of the IEFG and the EFG methods under different node distributions, we only change the parameters of the EFG method. When the EFG method is used, 8×8 regular nodes and 7×7 integral grids are selected, respectively, $d_{max} = 1.27$, $\alpha = 1.4 \times 10^3$, thus the smaller relative error is 0.2274%, and the CPU time is 0.23 s. Figs. 19–20 show the comparison of numerical solutions and analytical ones. It is shown that the IEFG method has higher numerical accuracy under the condition of more nodes distribution with more computational resources.

Figure 19: The comparison of numerical solutions and analytical ones along x_1-axis

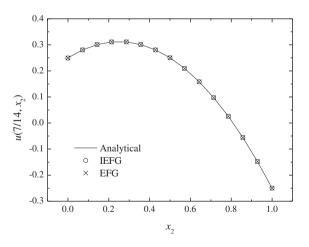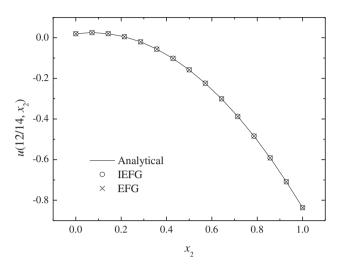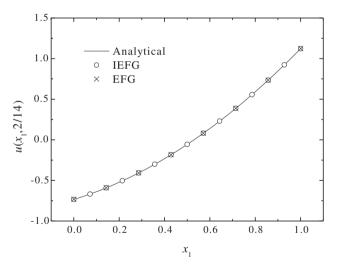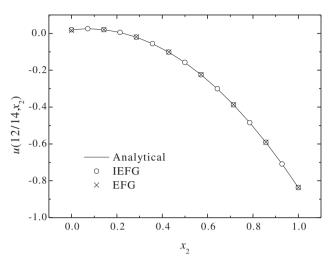**Figure 20:** The comparison of numerical solutions and analytical ones along x_2-axis

5 Conclusions

In this paper, we considered the IEFG method for solving 2D anisotropic steady-state heat conduction problems.

From Section 4, the good convergence of the solutions of the IEFG method is verified numerically. Moreover, the IEFG method can solve anisotropic steady-state heat conduction problems with less computational resources, and can be considered as a competitive alternative for solving science and engineering problems.

Therefore, the study in this paper can broaden the scope of application of the IEFG method.

Conflicts of Interest: The authors declare that they have no conflicts of interest to report regarding the present study.

References

1. Ahmadi, I., Sheikhy, N., Aghdam, M. M., Nourazar, S. S. (2010). A new local meshless method for steady-state heat conduction in heterogeneous materials. *Engineering Analysis with Boundary Elements, 34(12),* 1105–1112. DOI 10.1016/j.enganabound.2010.06.012.

2. Sun, L. L., Chen, W., Zhang, C. Z. (2013). A new formulation of regularized meshless method applied to interior and exterior anisotropic potential problems. *International Journal of Heat and Mass Transfer, 37(12–13),* 7452–7464. DOI 10.1016/j.apm.2013.02.036.

3. Ooi, E. H., Ooi, E. T., Ang, W. T. (2015). Numerical investigation of the meshless radial basis integral equation method for solving 2D anisotropic potential problems. *Engineering Analysis with Boundary Elements, 53,* 27–39. DOI 10.1016/j.enganabound.2014.12.004.

4. Gu, Y., Chen, W., Zhang, C. Z., He, X. Q. (2015). A meshless singular boundary method for three-dimensional inverse heat conduction problems in general anisotropic media. *International Journal of Heat and Mass Transfer, 84,* 91–102. DOI 10.1016/j.ijheatmasstransfer.2015.01.003.

5.   Reutskiy, S. Y. (2016). A meshless radial basis function method for 2D steady-state heat conduction problems in anisotropic and inhomogeneous media. *Engineering Analysis with Boundary Elements, 66,* 1–11. DOI 10.1016/j.enganabound.2016.01.013.

6.   Li, S., Liu, W. K. (2004). *Meshfree particle methods.* Germany: Springer-Verlag.

7.   Liu, W. K., Jun, S., Li, S. F., Adee, J., Belytschko, T. (1995). Reproducing kernel particle methods for structural dynamics. *International Journal of Numerical Methods for Engineering, 38,* 1655–1679. DOI 10.1002/nme.1620381005.

8.   Liu, W. K., Li, S. F., Belytschko, T. (1997). Moving least-square reproducing kernel method. (I) Methodology and convergence. *Computer Methods in Applied Mechanics and Engineering, 143,* 113–154. DOI 10.1016/S0045-7825(96)01132-2.

9.   Li, S. F., Liu, W. K. (1999). Reproducing kernel hierarchical partition of unity, Part I-Formulations and theory. *International Journal for Numerical Methods in Engineering, 45(3),* 251–288.

10. Belytschko, T., Lu, Y. Y., Gu, L. (1994). Element-free Galerkin methods. *International Journal for Numerical Methods in Engineering, 37(2),* 229–256. DOI 10.1002/nme.1620370205.

11. Lancaster, P., Salkauskas, K. (1981). Surface generated by moving least squares methods. *Mathematics of Computation, 37(155),* 141–158. DOI 10.1090/S0025-5718-1981-0616367-1.

12. Cheng, Y. M., Chen, M. J. (2003). A boundary element-free method for linear elasticity. *Acta Mechanica Sinica, 35(2),* 181–186.

13. Cheng, H., Zheng, G. D. (2020). Analyzing 3D advection-diffusion problems by using the improved element-free Galerkin method. *Mathematical Problems in Engineering, 2020,* 4317538. DOI 10.1155/2020/4317538.

14. Yu, S. Y., Peng, M. J., Cheng, H., Cheng, Y. M. (2019). The improved element-free Galerkin method for three-dimensional elastoplasticity problems. *Engineering Analysis with Boundary Elements, 104,* 215–224. DOI 10.1016/j.enganabound.2019.03.040.

15. Zheng, G. D., Cheng, Y. M. (2020). The improved element-free Galerkin method for diffusional drug releas e problems. *International Journal of Applied Mechanics, 12(8),* 2050096. DOI 10.1142/S1758825120500969.

16. Ren, H. P., Cheng, Y. M., Zhang, W. (2010). Researches on the improved interpolating moving least-squares method. *Chinese Journal of Engineering Mathematics, 27(6),* 1021–1029.

17. Ren, H. P., Cheng, Y. M. (2012). The interpolating element-free Galerkin (IEFG) method for two-dimensional potential problems. *Engineering Analysis with Boundary Elements, 36(5),* 873–880. DOI 10.1016/j.enganabound.2011.09.014.

18. Wu, Q., Liu, F. B., Cheng, Y. M. (2020). The interpolating element-free Galerkin method for three-dimensional elastoplasticity problems. *Engineering Analysis with Boundary Elements, 115,* 156–167. DOI 10.1016/j.enganabound.2020.03.009.

19. Wu, Q., Peng, P. P., Cheng, Y. M. (2021). The interpolating element-free Galerkin method for elastic large deformation problems. *Science China Technological Sciences, 64(2),* 364–374. DOI 10.1007/s11431-019-1583-y.

20. Cheng, Y. M., Bai, F. N., Liu, C., Peng, M. J. (2016). Analyzing nonlinear large deformation with an improved element-free Galerkin method via the interpolating moving least-squares method. *International Journal of Computational Materials Science and Engineering, 5(4),* 1650023. DOI 10.1142/S2047684116500238.

21. Qin, Y. X., Li, Q. Y., Du, H. X. (2017). Interpolating smoothed particle method for elastic axisymmetrical problem. *International Journal of Applied Mechanics, 9(2),* 1750022. DOI 10.1142/S1758825117500223.

22. Wang, J. F., Sun, F. X., Cheng, Y. M. (2012). An improved interpolating element-free Galerkin method with nonsingular weight function for two-dimensional potential problems. *Chinese Physics B, 21(9),* 090204. DOI 10.1088/1674-1056/21/9/090204.

23. Liu, F. B., Cheng, Y. M. (2018). The improved element-free Galerkin method based on the nonsingular weight functions for elastic large deformation problems. *International Journal of Computational Materials Science and Engineering, 7(4),* 1850023. DOI 10.1142/S2047684118500239.

24. Liu, F. B., Wu, Q., Cheng, Y. M. (2019). A meshless method based on the nonsingular weight functions for elastoplastic large deformation problems. *International Journal of Applied Mechanics, 11(1),* 1950006. DOI 10.1142/S1758825119500066.

25. Liu, F. B., Cheng, Y. M. (2018). The improved element-free Galerkin method based on the nonsingular weight functions for inhomogeneous swelling of polymer gels. *International Journal of Applied Mechanics, 10(4),* 1850047. DOI 10.1142/S1758825118500473.

26. Meng, Z. J., Cheng, H., Ma, L. D., Cheng, Y. M. (2018). The dimension split element-free Galerkin method for three-dimensional potential problems. *Acta Mechanica Sinica, 34(3),* 462–474. DOI 10.1007/s10409-017-0747-7.

27. Meng, Z. J., Cheng, H., Ma, L. D., Cheng, Y. M. (2019). The dimension splitting element-free Galerkin method for 3D transient heat conduction problems. *Science China Physics, Mechanics & Astronomy, 62(4),* 040711. DOI 10.1007/s11433-018-9299-8.

28. Meng, Z. J., Cheng, H., Ma, L. D., Cheng, Y. M. (2019). The hybrid element-free Galerkin method for three-dimensional wave propagation problems. *International Journal for Numerical Methods in Engineering, 117(1),* 15–37. DOI 10.1002/nme.5944.

29. Ma, L. D., Meng, Z. J., Chai, J. F., Cheng, Y. M. (2020). Analyzing 3D advection-diffusion problems by using the dimension splitting element-free Galerkin method. *Engineering Analysis with Boundary Elements, 111,* 167–177. DOI 10.1016/j.enganabound.2019.11.005.

30. Cheng, H., Peng, M. J., Cheng, Y. M. (2018). The dimension splitting and improved complex variable element-free Galerkin method for 3-dimensional transient heat conduction problems. *International Journal for Numerical Methods in Engineering, 114(3),* 321–345. DOI 10.1002/nme.5745.

31. Cheng, H., Peng, M. J., Cheng, Y. M. (2017). A hybrid improved complex variable element-free Galerkin method for three-dimensional potential problems. *Engineering Analysis with Boundary Elements, 84,* 52–62. DOI 10.1016/j.enganabound.2017.08.001.

32. Cheng, H., Peng, M. J., Cheng, Y. M. (2017). A fast complex variable element-free Galerkin method for three-dimensional wave propagation problems. *International Journal of Applied Mechanics, 9(6),* 1750090. DOI 10.1142/S1758825117500909.

33. Cheng, H., Peng, M. J., Cheng, Y. M. (2018). A hybrid improved complex variable element-free Galerkin method for three-dimensional advection-diffusion problems. *Engineering Analysis with Boundary Elements, 97,* 39–54. DOI 10.1016/j.enganabound.2018.09.007.

34. Cheng, H., Peng, M. J., Cheng, Y. M., Meng, Z. J. (2020). The hybrid complex variable element-free Galerkin method for 3D elasticity problems. *Engineering Structures, 219,* 110835. DOI 10.1016/j.engstruct.2020.110835.

35. Peng, P. P., Wu, Q., Cheng, Y. M. (2020). The dimension splitting reproducing kernel particle method for three-dimensional potential problems. *International Journal for Numerical Methods in Engineering, 121,* 146–164. DOI 10.1002/nme.6203.

36. Peng, P. P., Cheng, Y. M. (2020). Analyzing three-dimensional transient heat conduction problems with the dimension splitting reproducing kernel particle method. *Engineering Analysis with Boundary Elements, 121,* 180–191. DOI 10.1016/j.enganabound.2020.09.011.

37. Peng, P. P., Cheng, Y. M. (2021). Analyzing three-dimensional wave propagation with the hybrid reproducing kernel particle method based on the dimension splitting method. *Engineering with Computers.* DOI 10.1007/s00366-020-01256-9.

38. Peng, P. P., Cheng, Y. M. (2021). A hybrid reproducing kernel particle method for three-dimensional advection-diffusion problems. *International Journal of Applied Mechanics, 13,* 2150085. DOI 10.1142/S175882512150085X.

39. Wang, J. F., Sun, F. X. (2020). A hybrid generalized interpolated element-free Galerkin method for stokes problems. *Engineering Analysis with Boundary Elements, 111,* 88–100. DOI 10.1016/j.enganabound.2019.11.002.

40. Shiah, Y. C., Tan, C. L. (1997). BEM treatment of two-dimensional anisotropic field problems by direct domain mapping. *Engineering Analysis with Boundary Elements, 20,* 347–351. DOI 10.1016/s0955-7997(97)00103-3.

41. Luo, X., Huang, J. (2014). High-accuracy quadrature methods for solving boundary integral equations of steady-state anisotropic heat conduction problems with Dirichlet conditions. *International Journal of Computer Mathematics, 91(5),* 1097–1121. DOI 10.1080/00207160.2013.828050.